DOI 10.1007/s11182-019-01867-w

Russian Physics Journal, Vol. 62, No. 8, December, 2019 (Russian Original No. 8, August, 2019)

PECULIARITIES OF STRUCTURE FORMATION IN COPPER/STEEL BIMETAL FABRICATED BY ELECTRON-BEAM ADDITIVE TECHNOLOGY

K. S. Osipovich, A. V. Chumaevskii, A. A. Eliseev, K. N. Kalashnikov, E. A. Kolubaev, V. E. Rubtsov, and E. G. Astafurova

UDC 538.911: 621.521: 538.951

In the present paper, the microstructure of heterogeneous material bimetal compound fabricated by wire-feed electron-beam additive technology from CrNiTi *stainless steel and C11000 copper has been investigated. The bimetallic compound is characterized by the well-defined interface between the two materials and possesses two-phase transition areas on both sides of the interface. The heterogeneity of strength properties (microhardness) in the transition zones is associated with a solid solution hardening of the bimetal basis components and formation of composite structures in the transition zone of the bimetal: spherical inclusions of steel in the copper part and copper inclusions in the steel section. In the copper part of the bimetal sample, a heterogeneous grain structure is formed – areas with macroscale non-equiaxed grain structure and zones with spherical grains were observed. The heterogeneity of grain structure does not have significant influence on the yield strength, but affects the macroscopic deformation pattern of the bimetal copper part, as has been revealed by microstructural analysis of slip traces and grain structure calculated using the Hall–Petch relationship.*

Keywords: bimetal, stainless steel, copper, grain structure, electron beam additive manufacturing, 3D printing, mechanical properties.

INTRODUCTION

The development of scientific basis of structure formation of metals and alloys using additive manufacturing (AM) is one of the most urgent problems at this time in the field of condensed state physics and materials science. Materials scientists are interested in extending the range of materials that can be used to manufacture qualitative and defectless products of additive manufacturing, and physicists are interested in obtaining scientific knowledge on the structure formation of these materials on different scale levels. At present there is a wide range of materials fabricated using AM technologies, including steels [1, 2], aluminum [3, 4], titanium [5–7], nickel-based superalloys [8], and other metal materials [9]. The AM can also be effectively used to obtain bimetal products conventionally fabricated by welding or arc surfacing [10, 11].

Copper-steel bimetal is a typical multipurpose material, which can be widely applied in power generation and transmission industries, heat transfer components, cryogenic sector, bimetallic die-casting industry, etc. [12, 13]. At present, there are few works that study properties of copper-steel bimetals, which is caused by the complexity of

Institute of Strength Physics and Materials Sciences of the Siberian Branch of the Russian Academy of Sciences, Tomsk, Russia, e-mail: osipovich_k@ispms.tsc.ru; tch7av@gmail.com; alan@ispms.tsc.ru; sso.spektr.asu@gmail.com; eak@ispms.tsc.ru; rvy@ispms.ru; elena.g.astafurova@gmail.com. Translated from Izvestiya Vysshikh Uchebnykh Zavedenii, Fizika, No. 8, pp. 166–174, August, 2019. Original article submitted June 25, 2019.

TABLE 1. Chemical Composition of the Steel Substrate and the Copper Wire Used in this Work

Material	Chemical element (weight %)							
	Fe	Cu	Ni	Cr	Mn	Si	Cu	C
AISI 321	~67	–	8–9.5	17–19	up to 2	up to 0.8	up to 0.3	up to 0.12
C11000	up to 0.005	99.9	up to 0.002	–	–	–	–	–

fabrication of such bimetal compounds because of dissimilar physical and chemical properties of copper and steel. The Fe–Cu phase diagram has no intermetallic phases, except for a small area of limited solubility between Cu and Fe [14]. High reflectivity and low absorption of copper hinder the steel deposition on copper. High copper thermal conductivity equal to 401 W/(m·deg) dissipates heat rapidly away from the molten pool, which hinders reaching the melting temperature [14]. The significant difference of thermal expansion coefficients and thermal conductivities between copper and steel inevitably cause large misfit strain and residual stresses in the joint leading to solidification cracks [14]. Hydrogen is highly soluble in liquid copper and normally could form pores at bonding region [14]. Thus, the problem of bonding of diverse metals has not yet been solved by the present time. We have not succeeded in finding experimental or theoretical works devoted to investigation of the microstructure and physical properties of copper-steel bimetals fabricated by the AM in the open literature. Nevertheless, the method of wire-feed electron beam 3D-printing has a number of technological features that are promising for fabrication of bimetal compounds, including copper-iron ones: vacuum printing conditions, high energy consumption, and high electron beam power.

The purpose of the present work is to establish the peculiarities and mechanisms of microstructure formation in various areas of the copper and austenite steel bimetallic sample fabricated by the wire-feed electron-beam 3D-printing.

1. EXPERIMENTAL TECHNOLOGY

Samples were fabricated using a laboratory experimental equipment for electron beam additive manufacturing of metal products. For 3D printing of samples, a copper C11000 wire with a diameter of 1 mm surfaced on a rectangular stainless steel AISI 321 substrate 3 mm thick was chosen. The Chemical composition of the employed materials is given in Table 1.

The molten pool was formed by an electron beam in a vacuum atmosphere on the stainless steel substrate fixed on a movable three-axis water-cooled table. 3D printing of a vertical wall was carried out by level-by-level deposition of the material. In the beginning of each new layer, the table was returned at the starting position with correction of its height. Two strategies of electron beam 3D printing were chosen. In the first case (strategy I), 15 wire layers were continuously deposited. In the second case (strategy II), after deposition of the seventh layer, 3D printing was compulsory stopped to cool the entire wall, then wire deposition was continued again before fabrication of the finished 15-layer sample. The finished samples represented vertical walls with length of ≈80 mm, thickness of ~8 mm, and height of 20 mm. To study the microstructure and mechanical properties, the samples were cut from the vertical walls grown on an electrical discharge machine DK7750 (Fig. 1).

To study the grain structure and the elemental composition of the bimetal and to measure its microhardness, the samples with flat cross sections were cut from the grown walls. To investigate the microstructure of the copper part of the bimetal and to perform tensile tests, double blades with linear sizes 2.5 × 2.1 × 12 mm were cut from the samples so that the tensile axis coincided both with the layer deposition direction and with the wall growth direction. Before microstructural analysis, the samples were grinded and polished with a diamond paste. To study the copper grain structure, the polished sample surfaces were etched in the solution 10 ml HCl + 1 g FeCl + 20 ml H_2O.

The metallographic analysis of the sample structure was performed with a confocal OLYMPUS LEXT OLS4100 microscope. The uniaxial static tensile tests of mechanical properties of the samples were performed at room temperature with initial strain rate of $1.4 \cdot 10^{-3}$ s^{-1} using a universal UTS 110M-100 1-U testing machine. To determine the elemental composition of the samples, a SEMTRACK mini scanning electronic microscope equipped with an attachment for energy dispersive elemental microanalysis was used.

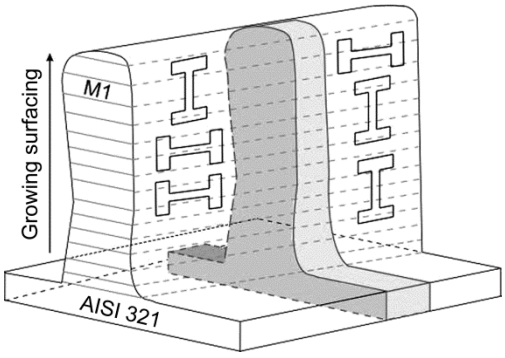

Fig. 1. Schematic of samples cut from the grown vertical wall produced by the method of wire-feed electron-beam 3D-printing. The areas corresponding to the initial material structure are hatched.

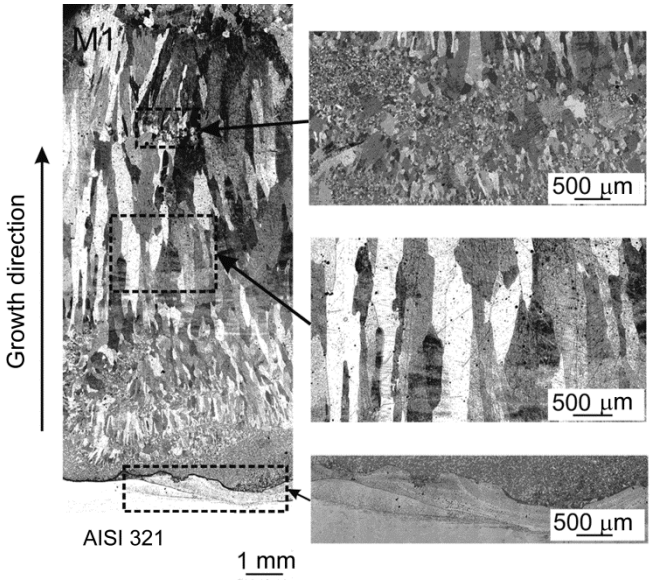

Fig. 2. Light microscopy image of the microstructure of the sample grown by strategy I. The arrows indicate the magnified images of the steel-copper interface and areas with nonequilibrium large spherical grains in the copper part of the bimetal.

2. EXPERIMENTAL RESULTS AND DISCUSSION

Figure 2 shows metallographic images of the etched lateral surface of the bimetal copper – austenite steel sample grown by strategy I. An analysis of the image demonstrates that the bimetal from diverse materials – stainless steel and copper – has a well-defined interface. No cracking defects are observed along the interface, which testifies to the complete deposition of the layers. In this case, the shrink pores typically formed during deposition of the first layers of the material and in contact with the substrate were not observed.

The elemental composition of the near-interface area is illustrated by Fig. 3*a*. The content of elements on the left and on the right of the interface corresponded to the chemical composition of stainless steel 321 – copper C11000 substrate. In the plot of the dependence of the elemental composition on the distance to the interface (on the left

TABLE 2. Analysis of the Elemental Composition of the Near-Interface Area of the Copper-Steel Bimetal Compound

Area	Chemical element (wt %)			
	Fe	Cu	Ni	Cr
1	1.936	96.255	0.954	0.642
2	59.113	17.646	5.154	17.760
3	65.091	10.783	5.160	18.435

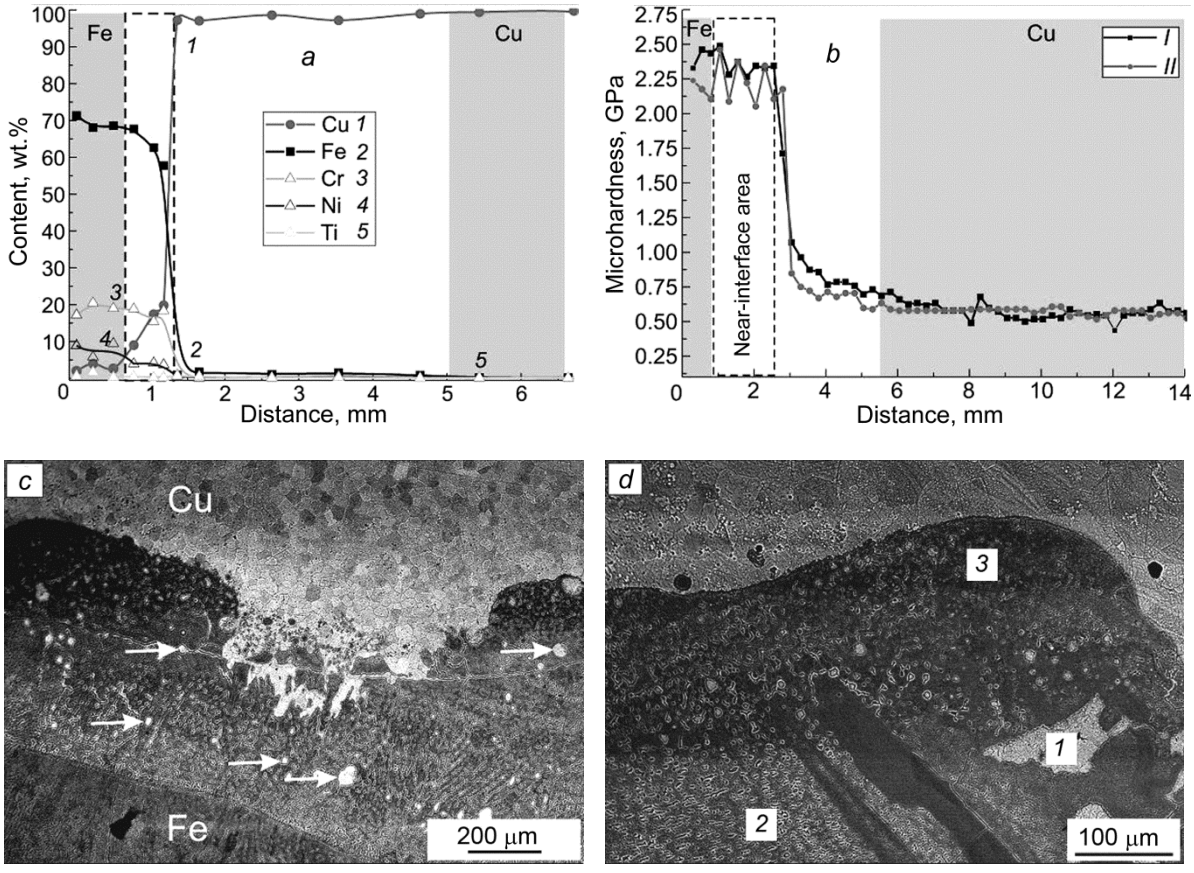

Fig. 3. Change in the elemental composition (*a*), microhardness (*b*) of samples grown by strategies I and II, and microstructures of the transitive bimetal layer (*c* and *d*). Areas with initial material structure (Fe – AISI 321, Cu – copper C11000) are shown in Fig. 3*a* and *b*. Areas for which the elemental composition was analyzed (Table 2) are labeled in Fig. 3*d*.

of the figure), a transitive zone with thickness 300–700 μm can be seen in which the austenite steel structure differed from that in Table 1 and sufficiently high concentration of copper was observed (Fig. 3*a*). A wide spread of microhardness values corresponded to this area in Fig. 3*b*; it clearly stands out in Fig. 3*c* showing a thin section of the etched sample.

In the transitive area, spherical copper inclusions (designated by the arrows in Fig. 3*c* and presented in Table 2) were observed; copper has enhanced etchability compared to the austenite steel substrate. An analysis of the data shown in Fig. 3 demonstrates that in the transitive zone, the austenite stainless steel is alloyed by copper atoms, and the biphase area – copper and austenite stainless steel alloyed with copper – is formed. This does not contradict to the phase Fe–Cu

state diagram [14, 15] according to which the iron and copper based intermetallic compounds are not formed, but a limited amount of copper (~5.8 %) may be dissolved in γ-Fe at a temperature of 1083°C [15]. The number of spherical copper inclusions decreased with increasing distance from the interface; hence, the copper concentration also decreased.

Near the interface, inclusions with weak etchability and morphology close to that of the austenite steel structure below the interface of the bimetal compound were also observed in the copper part of the bimetal (Fig. 3*c*). A small concentration of iron in the copper part of the bimetal sample near the interface can be caused by formation of the solid solution of iron in copper, though the solubility of iron in copper is rather low (~2.8 % at a temperature of 1083°C) [15]. At a distance of ~4 mm from the interface, the Cu content was 98.9 wt. %, which was close to the structure of copper C11000. No well-defined transitive zone testifying to the formation of solid solution of iron in copper was observed for thin metallographic sections. However, formation of relatively small copper grains near the transitive zone should be pointed out, whereas in the process of wall growth the non-equiaxed grain structure, testifying to directed crystallization in the process of additive growth, was observed with increasing distance from the interface. One of the factors promoting the formation of the equiaxed relatively small grains near the substrate can be alloying of copper with iron as well as with titanium, nickel, or chromium that present in austenite steels and promote formation of a considerable number of crystallization nuclei during cooling of the wall.

Thus, the phase structure of the bimetal austenite steel γ-Fe (Cr, Ni, Ti) – copper γ-Cu samples fabricated by the method of electron beam AM changes during transition through the section interface by the following sequence:

$$\text{γ-Fe (Cr, Ni, Ti)} \rightarrow \text{γ-Fe (Cr, Ni, Ti, Cu)} \rightarrow \text{γ-Fe (Cr, Ni, Ti, Cu)} + \text{γ-Cu, Fe}$$

$$\rightarrow \text{interface} \rightarrow \text{γ-Cu, Fe} + \text{γ-Fe (Cr, Ni, Ti, Cu)} \rightarrow \text{γ-Cu} + \text{γ-Cu, Fe} \rightarrow \text{γ-Cu}.$$

An analysis of the microhardness distribution during transition through the interface between the sections in a bimetal sample testifies to a sharp change in the strength properties of the material from 2.29 GPa corresponding to the austenite steel to 0.54 GPa in the copper part of the sample. For transitive zones near the interface between the sections described above, the spread of microhardness values (in the steel section of the bimetal) and the increased microhardness values (in the copper part of the bimetal) are observed (Fig. 3*b*). The spread of values in the steel section of the wall near the section interface is caused by the fact that during microhardness measurements, Vicker's pyramid pressed partly on soft copper inclusions in the transitive zone. In the copper part of the wall near the section interface, higher microhardness values in the transitive zone compared to the main bulk of copper C11000 can be caused by several factors: steel inclusions presented in the measurement (indentation) area; solid solution hardening of copper by iron; smaller grain sizes in the transitive zone compared to the main copper part of the wall.

As to the barrier effect (the effect of the grain size described by the Hall–Petch relationship), the copper part of the wall is of particular scientific interest. According to the microstructure shown in Fig. 2, after the transitive zone with small grain sizes, directed crystallization occurred in the copper part of the wall. It was accompanied by the growth of columnar grains elongated in the direction of wall growth. This is in agreement with the peculiarities of crystallization of many materials using the AM and can cause anisotropy of the mechanical properties of samples fabricated by the wire-feed electron-beam additive manufacturing [16]. Since the growth of the wall by strategy I occurred continuously, a homogeneous growth of large grains would be expected along the entire height of the wall. Nevertheless, the microstructural analysis reveals sufficiently extended areas with equiaxed copper grains. Such areas are located in the central and upper sections of the wall (Fig. 2). Since the elemental composition of the wall in these sections corresponds to the wire made of copper C11000, such special features of crystallization can be caused by heterogeneous heat removal from the wall during additive growth. To confirm this assumption, samples were grown by stage-by-stage strategy II of 3D electron-beam printing with additional intermediate stage of growth interruption during which the wall was cooled giving off heat through the substrate to the cooled table. After termination of the stage of intermediate growth interruption and cooling of the sample, fine-grained areas analogous to those of the sample grown by strategy I were formed in the central section of the wall in the beginning of the second growth stage. Then the directed growth of columnar grains was observed again when the growth process was continued (Fig. 3).

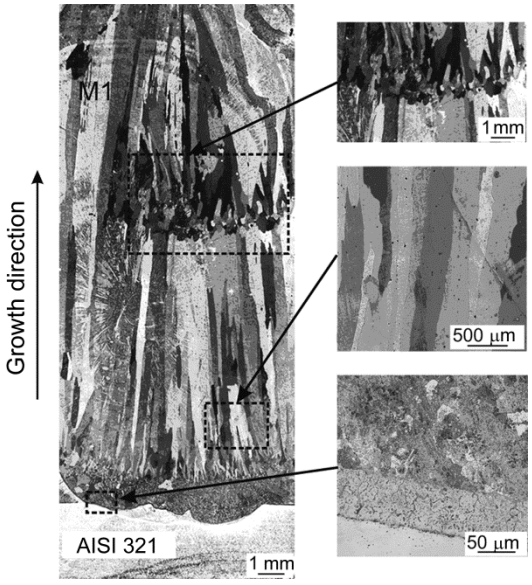

Fig. 4. Image of the microstructure of the sample grown by strategy II. The arrows indicate images of the steel-copper interface and areas with non-equiaxed large and spherical grains in the copper part of the bimetal.

To confirm this assumption, the samples were grown by three-stage strategy (II) of wire-feed electron-beam 3D printing. During forced cooling, analogous fine-grained areas were formed in the central section of the wall, and then during subsequent continuous growth, the directed growth of columnar grains was observed again (Fig. 4).

Hence, even during continuous growth of materials with low melting temperature and high heat conductivity such as copper, heterogeneities of the microstructure can be observed without continuous grain growth. During deposition of the first layers of copper C11000 on the substrate made of stainless steel 321, one grains grow at the expense of neighboring grains via migration of high-angle boundaries, that is, collective recrystallization is observed. In this case, the grain boundaries migrate, and the equilibrium structure with a minimal surface energy and grains of equal sizes and shapes is formed. The impurity atoms and inclusions of the second phase (in the transitive zone) promote formation of a great number of recrystallization nuclei, but hinder migration of grain boundaries. In the process of development of collective recrystallization, the driving force decreases, and the grain growth is stopped after achievement of a certain critical value. Thus, roundish grains which average size of 254 μm are formed during deposition of the first layers of copper C11000 on the AISI 321 stainless steel substrate. After collective recrystallization, secondary recrystallization occurs. In this case, favorably oriented grains grow, thereby forming crystallographic structure in the material. After termination of secondary recrystallization, anomalously large elongated grains are formed with average length and width equal to 3.5 and 0.3 mm, respectively. The temperature gradient plays a key role in morphology and size of the structure and defines the crystallization mode. During deposition of the first layers of copper C11000 on the steel 321 substrate, the heat is fast scattered that in combination with alloying of copper with austenite steels components (first of all, iron) and formation of inclusions of the second phase entails formation of fine-grained structure. The influence of these factors decreases with the growth of the wall, and the directed growth of the grain occurs. The directed growth of grains is promoted by a slow heat removal and by temperature gradients formed during additive growth of the wall.

Since substantially heterogeneous grain structure is formed in the copper part of the wall during additive growth of the bimetal, its mechanical properties can differ significantly from the properties of cast copper and may be anisotropic. Despite of the fact that the microhardness values are independent of the section of the wall in which they were measured (except the transitive zone), the mechanical properties can significantly depend on the deformation direction [16]. To establish the influence of the heterogeneity of the microstructure of the samples with different

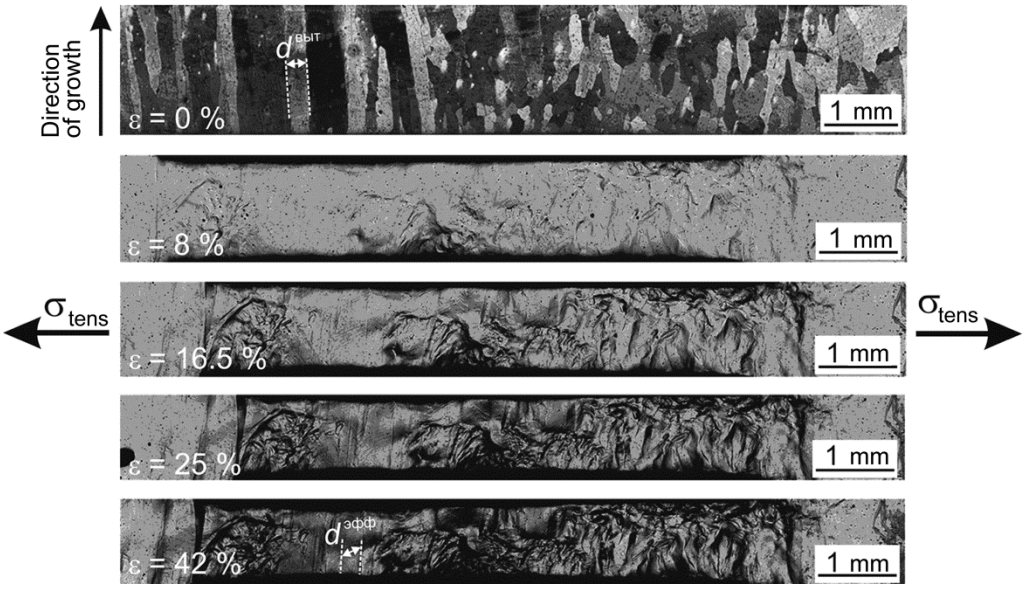

Fig. 5. Metallographic images of the surfaces of samples with the tensile axis perpendicular to the elongated grains for degrees of plastic strain indicated in the images.

directions of grains relative to the direction of tensile load application, an analysis of metallographic images of the sample surfaces with different degrees of plastic deformation was carried out (Figs. 5 and 6). In addition to columnar grains in the working sections of the samples, areas with equiaxed grains were also observed. For this reason, the plastic deformation and strain hardening of samples by the method of electron beam wire AM is developed macroscopically heterogeneously (Figs. 5 and 6). Irrespective of the orientation of non-equiaxed grains with respect to the tension direction and the grain sizes and shapes, plastic deformation was developed in all elements of the structure. The slip microbands characteristic for plastic deformation of coarse-grained copper (Figs. 5 and 6) are observed both in columnar grains and equiaxed slip lines [17].

Since the samples have the same structures and the mechanism of copper deformation is independent of the orientation of grains with respect to loading and is realized via dislocation slipping [18], the yield strength $\sigma_{0.2}$ is primarily determined by the grain size d (the free path length of sliding dislocations $a/2$ <110> in the grain) according to the Hall–Petch relationship [19]:

$$\sigma_T = \sigma_0 + K \cdot d^{-1/2},$$

where K = 0.11 MPa·m$^{-1/2}$ [20] is the Hall–Petch coefficient for copper and σ_0 = 13 MPa [18] is the yield stress in a single crystal (the friction stress of the lattice).

For samples with columnar grains oriented perpendicularly to the applied load, the average length of slip lines in columnar grains in Fig. 5 was 246 μm, and the average size of equiaxed grains was d^{eq} = 254 μm. Thus, according to the Hall–Petch relationship, the yield strength for grains of both types was about 20 MPa (Table 3). Hence, under application of tensile stresses in the direction perpendicular to the elongated grains, the plastic deformation of samples with heterogeneous structure was determined by the onset of slipping dislocation motion in non-equiaxed and in equiaxed grains practically simultaneously. The deformation tracks are seen in all grains in metallographic images starting from the early deformation degrees (Fig. 5).

TABLE 3. Grain Sizes and Yield Strengths Calculated from the Hall–Petch Relationship for Equiaxed ($\sigma_{0.2}^{equ}$) and Non-Equiaxed ($\sigma_{0.2}^{elong}$) Grains. The Sizes Correspond to the Microstructure of Samples under Tension

Samples	d^{equi}, μm	d^{elong}, μm*	d^{eff}, μm**	$\sigma_{0.2}^{equi}$, MPa	$\sigma_{0.2}^{elong}$, MPa
Tensile axis is perpendicular to elongated grains	254	203	246	19.9	20.0
Tensile axis is parallel to elongated grains	234	254	315	20.2	19.2

Notes. Here * indicates the minimal linear grain size (perpendicular to the columnar grains), and ** indicates the average length of slip lines in non-equiaxed columnar grains.

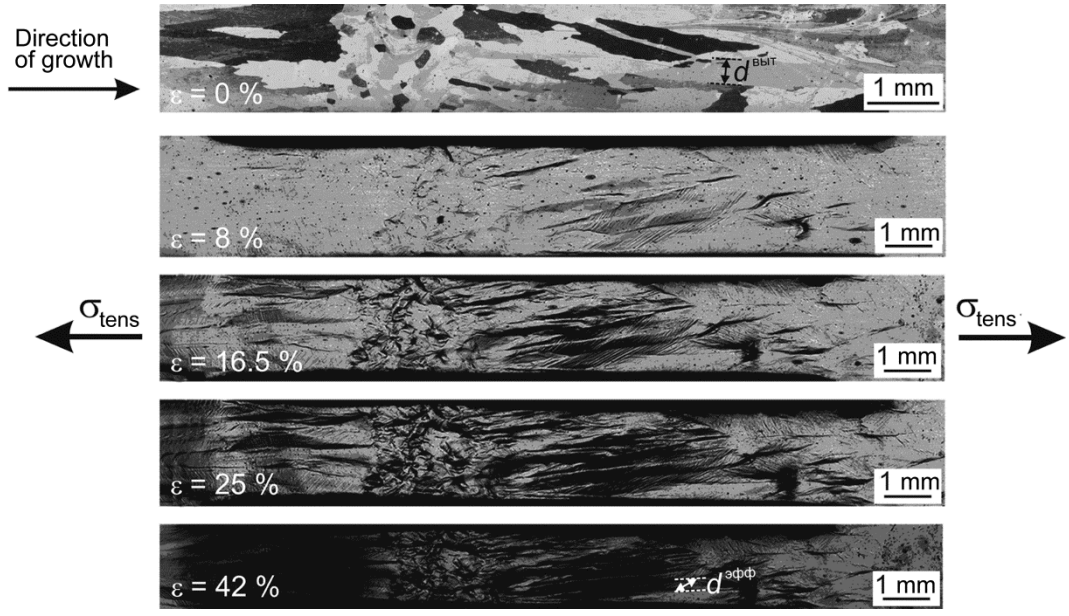

Fig. 6. Metallographic images of the surfaces of samples with the tensile axis parallel to the elongated grains for degrees of plastic strains indicated in the images.

The plastic deformation of the samples with the tensile axis parallel to the elongated grains develops also in grains of both types, because the stresses at which the plastic deformation starts in them are close in values despite of the difference in the grain sizes. The effective dislocation path length in elongated grains is slightly greater than in spherical grains (Table 3).

Thus, the heterogeneity of the grain structure, the directed crystallization, and the simultaneous presence of local areas with equiaxed fine grains have no considerable influence on the development of plastic deformation on the microstructural level in the copper part of the bimetal. The macroscopic heterogeneity of plastic flow experimentally observed in Figs. 5 and 6 is most likely caused by the influence of the grain boundaries on the peculiarities of macroscopic flow of additively grown copper crystals that requires independent research.

CONCLUSIONS

It has been shown experimentally that in the case of wire-feed electron-beam 3D printing of a bimetal sample of stainless steel 321 and copper C11000, the well-defined interface is formed that has macroscopically heterogeneous structure with transitive zones in copper and steel sections of the wall. In the steel section of the wall, the transitive zone

300–700 μm thick is formed with characteristic solid solution of copper in austenite steel and spherical inclusions of copper alloyed by iron. The formation of this composite structure in the transitive zone of the bimetal is accompanied by a wide spread of microhardness values. In the copper part of the transitive zone, increased values of microhardness observed experimentally are caused by the solid solution hardening of copper by austenite steel components (primarily iron) and formation of spherical inclusions of austenite steels alloyed by copper.

During growth of the bimetal sample (with increasing distance from the transitive zone), the non-equiaxed grain structure is formed, thereby testifying to the directed crystallization during additive growth of copper. Results of microstructural analysis of slip and grain tracks demonstrated that the heterogeneities in the grain shapes and sizes do not influence the onset of the plastic flow in copper. The yield stress calculated from the Hall–Petch relationship depends weakly on the grain shape and orientation with respect to external loading, and the sliding tracks are observed with a microscope in all grain types (spherical and non-equiaxed columnar). The heterogeneous grain structure formed during additive growth of the copper part of the bimetal sample influences the macroscopic deformation pattern, which is most likely caused by the influence of the orientation and density of grain boundaries in the section formed during additive growth of the bimetal.

This work was performed within the frame of the Fundamental Research Program of the State Academies of Sciences for 2013-2020, line of research III.23.

REFERENCES

1. S. Yu. Tarasov, A. V. Filippov, N. L. Savchenko, *et al*., Int. J. Adv. Manuf. Tech., **99**, 2353–2363 (2018).
2. H. D. Carlton, A. Haboub, G. F. Gallegos, *et al*., Mater. Sci. Eng. A, **651**, 406–414 (2016).
3. K. Schmidtke, F. Palm, and A. Hawkins, Phys. Procedia, **12**, 369–374 (2011).
4. E. Louvis, P. Fox, and C. J. Sutcliffe, Proc. Tech., **211**, 275–284 (2011).
5. K. Yamanaka, W. Saito, M. Mori, *et al*., Addit. Manuf., **8**, 105–109 (2015).
6. A. Yu. Nikonov, A. M. Zharmukhambetova, A. V. Ponomareva, *et al*., Phys. Mesomech., **21**, 43–50 (2018).
7. Y. Zhai, H. Galarraga, D. A. Lados, *et al*., Procedia Eng., **114**, 658–666 (2015).
8. P. Nie, O. A. Ojo, and Z. Li, Acta Mater., **77**, 85–95 (2014).
9. X. Z. Xin, N. Xiang, J. Chen, *et al*., Mater. Lett., **88**, 101–103 (2012).
10. T. Abe and H. Sasahara, Precis Eng., **45**, 387–395 (2016).
11. S. Meco, G. Pardal, and S. Ganguly, Opt. Lasers Eng., **67**, 22–30 (2015).
12. J. Kar, S. K. Roy, G. G. Roy, *et al*., Mater. Process. Technol., **233**, 174–185 (2016).
13. O. M. Al-Jamal, S. Hinduja, and L. Li, CIRP Ann., **57**, 239–242 (2008).
14. C. Tana, K. Zhoua, W. Ma, *et al*., Mater. Design, **155**, 77–85 (2018).
15. S. V. Shukhardin, ed., Bi- and Multicomponent Copper-Based Systems [in Russian], Nauka, Moscow (1979).
16. P. Åkerfeldt, M.-L. Antti, and R. Pederson, Mater. Sci. Eng. A, **674**, 428–437 (2016).
17. É. V. Kozlov, N. A. Konev, A. N. Zhdanov, *et al*., Fizich. Mesomekh., **4**, 93–113 (2004).
18. É. V. Kozlov, A. N. Zhdanov, L. N. Ignatenko, *et al*., in: Ultrafine Grained Materials II, Warrendale, TMS (2012), pp. 419–428.
19. T. H. Johnston and C. E. Feltner, Metall. Trans., **1**, 1161–1167 (1970).
20. A. M. Glezer, Principles of Plastic Deformation of Nanostructural Materials [in Russian], Fizmatlit, Moscow (2016).